Cell-imprinted-based integrated microfluidic device for biomedical applications: Computational and experimental studies

Sepideh Yazdian Kashani
Amirkabir University of Technology
Mostafa Keshavarz Moraveji (moraveji@aut.ac.ir)
Amirkabir University of Technology
Shahin Bonakdar
Pasteur Institute of Iran

Research Article

Keywords: Cell-imprinted substrate, Microfluidics, Computational fluid dynamic, Biomedical application, Chondrocyte, Stem cell differentiation

Posted Date: March 11th, 2021

DOI: https://doi.org/10.21203/rs.3.rs-270275/v1

Abstract

It has been proved that cell-imprinted substrates molded from template cells can be used for the re-culture of that cell while preserving its normal behavior or to differentiate the cultured stem cells into the template cell. In this study, a microfluidic device was presented to modify the previous irregular cell-imprinted substrate and increase imprinting efficiency by regular and objective cell culture. First, a cell-imprinted substrate from template cells was prepared using a microfluidic chip in a regular pattern. Another microfluidic chip with the same pattern was then aligned on the cell-imprinted substrate to create a chondrocyte-imprinted-based integrated microfluidic device. Computational fluid dynamics (CFD) simulations were used to obtain suitable conditions for injecting cells into the microfluidic chip before performing experimental evaluations. In this simulation, the effect of input flow rate, number per unit volume, and size of injected cells in two different sizes of the chip were examined on exerted shear stress and cell trajectories. This numerical simulation was first validated with experiments with cell lines. Finally, chondrocyte was used as template cell to evaluate the chondrogenic differentiation of adipose-derived mesenchymal stem cells (ADSCs) in the chondrocyte-imprinted-based integrated microfluidic device. ADSCs were positioned precisely on the chondrocyte patterns, and without using any chemical growth factor, their fibroblast-like morphology was modified to the spherical morphology of chondrocytes after 14 days of culture. Both immunostaining and gene expression analysis showed improvement in chondrogenic differentiation compared to traditional imprinting methods. This study demonstrated the effectiveness of the cell-imprinted-based integrated microfluidic devices for biomedical applications.

1. Introduction

It has been proven that cells' natural environment effectively controls cells' function, and cells lose their normal behavior after isolating themselves from their natural environment [1–3]. For example, chondrocytes' spherical morphology will be lost after a mono-layer culture on a polystyrene plate, and they will gain fibroblast-like morphology [4]. Also, providing healthy chondrocytes from the patient or donor and in vitro culture for knee osteoarthritis treatment is one of the most common non-fatal diseases, which is expected to increase dramatically in the coming decades among the world population, is challenging [2, 3]. In order to overcome the limitations of using chondrocytes, many researchers have been gradually attracted to adipose-derived mesenchymal stem cells (ADSCs), which can be differentiated for generating cartilage [1, 2, 4, 5].

Therefore, in regenerative medicine based on stem cell manipulation, researchers try to imitate the cells' natural environment by creating similar conditions for their growth and differentiation. The extracellular matrix (ECM), as a supportive structure for a cell, provides the physical, chemical, and mechanical conditions for cell adhesion, growth, and differentiation [5]. Morphological structure and mechanical loading change cell fate during growth in the embryonic period [6]. The traditional substrate for cultivating cells in a laboratory is made of transparent and hydrophobic polystyrene. However, this substrate's rigidity induces a hard tissue, like the bone, in cells and, therefore, increases the osteogenic differentiation

probability [7]. The role of culture substrate in cellular behavior has been evaluated in several studies [8–11]. Researches have shown that stem cells' shape and synthetic extracellular matrices can control their fate [12–17]. Also, the researches confirm the importance of surface topography for stem cell differentiation [18–23].

The method of inducing differentiation in stem cells through cell shape engineering (imprinting) was first implemented by Mahmoudi et al.[2]. A cell-imprinted substrate was fabricated from the chondrocyte shape as a physical stimulus for inducing chondrogenic differentiation in stem cells. Moreover, the imprinting method can enhance cardiomyogenic differentiation efficiency in induced pluripotent stem cells [24]. Tenogenic, osteogenic, kertainogenic, and Schwann cell differentiation in stem cells were also obtained with the imprinting method [25–29]. Also, the effect of physical topography on the cancer cells' response to the conventional anti-cancer drugs was investigated in [30]. Cancer bioimprinting and cell shape recognition can improve detection limits or eliminate the need for a thorough patient samples analysis. [31]. So, the cell-imprinted substrate can manipulate cell phenotypes and regulate their function [24,32]. However, this process's efficacy is poor because of the lack of control over the cells' location.

The rapid development of microfluidic technology is a way of mimicking an in vivo-like microenvironment [33–36]. The primary purpose of producing microstructures is to convert today's complicated and costly laboratories into fast, inexpensive, and high-efficient micro-scale laboratories [37,38]. This technology can provide and transport cell culture medium and even air, while the waste products by cellular activities are discharged like the human circulatory system. Microfluidic devices' other benefits are biocompatibility, high surface-area-to-volume ratio, continuous and homogenous feeding of cells, automated cell culture media perfusion, and ease of handling. Moreover, they provide spatial-temporal control on the microenvironment scale (0.1–100 μm). Microfluidic devices are used with the controlled microenvironment to investigate the effects of external factors on cell fate [39–45].

Therefore, many research efforts are now focused on using microfluidic devices for cell culture studies in developing medicines and biological research applications, such as drug toxicity or metabolism studies also for stem cell research [33,37,46–49]. Specifically, the organ on a chip concept has attracted researchers, which is a microfluidic cell culture platform consisting of a continuous perfusion system with living cells that can mimic the tissue or organ [50]. Stem cell culture and differentiation require careful control of several cell culture microenvironment signals regulating intracellular signaling and, eventually, cell phenotype. The development of such precise monitoring is difficult for traditional cell culture systems [40, 54]. In addition, in comparison with conventional methods, microfluidic systems can simultaneously combine physical and biochemical factors to provide precise and repeatable stimulation for controlled stem cell differentiation, which is very important in regenerative medicine [33,51–59].

A hybrid microfluidic system was developed by putting aligned polydimethylsiloxane (PDMS) microgrooves on the surface of biodegradable polymers as physical cues for regulating hiPSC neural differentiation and creating a dynamic microenvironment. Neuronal-specific gene expression on the

microfluidic device was shown to be considerably higher than traditional systems: an indicator of improved differentiation of hiPSCs into neuronal cells in the microfluidic device [58].

In traditional imprinting methods, the template cells have entirely random placement, so the secondary cell's probability of being placed exactly on the first cell template is low. Therefore, herein to increase the traditional imprinting methods efficiency, a microfluidic-based platform is introduced. The template cells are first cultured in a microfluidic chip on a cell culture plate in this method. Their topography is transferred to a silicone replica by mold casting in a regular pattern. The regular cell-imprinted pattern is then used as a second culture substrate under the other microfluidic chip aligned to the regular cells pattern. The cell culture environment is both predictable and controllable since the entire process is performed inside the chips.

Furthermore, cells' culture is dynamic, and the cell culture medium passes continuously over cells, which mimics the fluidic flow like in the body. Using a micrometer level cell-imprinted-based integrated microfluidic device reduces the number of cells needed in one experiment. It introduces the sufficiently accurate, reproducible, and low-cost substitute of traditional cell culture plates to control cells' fate. This procedure can be used in cell therapy or drug analysis while preserving normal cell activity or stem cell differentiation into target cells.

Although these experimental methods are reliable, they are very time-consuming to characterize the fluid flow in a microfluidic cell chip. Computational fluid dynamics (CFD) is a powerful tool for overcoming these limitations and enables complete characterization of flow fields. The design of microfluidic cell culture systems and, therefore, their associated flow and patterns can be theoretically evaluated before construction. Certain parameters such as fluid inlet velocity and its effect on shear stress applied to cells or injection cell concentrations and its effect on filling microfluidic chip microchannels can also be evaluated to predict their effect better and obtain appropriate conditions before entering the laboratory and testing on cells. In fact, we will have a virtual lab that will save time and reduce the cost.

Therefore, in this study, numerical evaluations of fluid flow and cell tracing in the microfluidic chip were performed and validated with an experimental assessment on cell lines. The appropriate conditions of cell injection that have been found through simulation were used to prepare the chondrocyte-imprinted substrate. After chondrogenic differentiation of stem cells, in vitro assessments such as immunocytotoxicity and real-time PCR were done.

2. Material And Methods

2.1 Microfluidic chip design

The location of the template cells should be monitored to improve the efficiency of the imprinting process, so a set of 128 micro-channels (20 mm length and 50 μm depth) microchannels with a width of 25 μm and 40 μm comparable to that of template cells have been considered (Fig. 1.a and FigS1.a).

Approximately 2×10^6 cells (with an average diameter of 8 μm) can be placed in regular and parallel lines in a microfluidic chip with 40 μm microchannels. At the end of each microchannel, three diamond-shaped microposts were considered to inhibit cells' removal from their ends during cell injection. These microposts limited the available space's width to 2 μm per side of the microchannel for moving cells while providing the cell culture medium exchange (Fig. 1.d). The input channel's width is 0.6 mm and 0.96 mm in the chip with 25 μm and 40 μm microchannels, respectively.

2.2 Computational fluid dynamics analysis

Computational fluid dynamics (CFD) modeling is a useful technique that has been used in the field of microscale cell culture. It allows a deeper understanding of the function of the hydrodynamic environment and the factors that regulate it. CFD is generally applied to chemical and mechanical engineering; recently, it is used to consider the effects of fluid flow on cell function and offers valuable insights into microfluidic cell culture chip design and optimization. Thus, before fabrication, microfluidic cell culture device designs and their respective flow rates and patterns can be theoretically evaluated and characterized. Further precise parameters such as fluid inlet velocities and channels dimension can also be varied to better predict their effect on shear stresses, thus optimizing cell growth conditions [35,37,60,61].

So in this study, to better understand the microfluidic chip's flow characteristics, a numerical simulation of the microchip was computed using the COMSOL Multiphysics software. For the simulation, a 2D creeping flow model based on the steady-state Navier-Stokes' equation and the particle tracing model for fluid flow were used. An in-compressible fluid with 1000 kg/m^3 density and 0.001 Pa.s dynamic viscosity, were considered.

The boundary conditions of inlet velocity and zero pressure were used at the inlet and outlet, respectively, and no-slip conditions were applied to all walls. Particles were released in random position at the chip's inlet with a coupling velocity of the creeping flow model, and in the particle tracing model, drag force based on Stokes' equation was applied. For the initial assessment, the injection flow rate of 2.12 ml/h for syringe pump (equivalent to 0.012291 m/s and 0.019666 m/s inlet velocities in the chip with 40 μm and 25 μm microchannels respectively) and 2×10^6 cells in 170 μl of culture medium with an average diameter of 12 μm and normal distribution of particles were considered.

A convergence and mesh independence study was performed for various mesh sizes to investigate mesh element number effect on average shear stress and velocity in the whole chip surface (Fig. 1.b-c and FigS1.b-c). The final mesh with minimum element qualities of 0.21 and 0.27 and average element qualities of 0.74 and 0.69 was selected for the chips with 40 μm and 25 μm microchannels, respectively (Fig. 1.d and FigS1.d). As shown in the figures, the percentage error with the converged value can be ignored for the selected mesh. Therefore, the selected mesh provides the answer with high accuracy and appropriate calculation time. Finer mesh has been used in the areas around the microposts, which have increased velocities due to reduced passage width. After the appropriate mesh selection, the fluid flow and cells tracing model inside the microfluidic chip were solved. Also, various parameters such as fluid inlet velocity, number of cells, and cells' sizes were changed to obtain suitable laboratory conditions. First,

the results of this study were verified by experimental evaluations on cell lines. The appropriate values for cell concentration per unit volume of cell culture medium and injection flow rate of syringe pump chosen based on simulation results were then used to prepare chondrocyte-imprinted substrate and future stem cells chondrogenic differentiation in a cell-imprinted-based integrated microfluidic device.

2.3 Experimental analysis

2.3.1 Cell culture

All the experiments were approved by the ethics committee of the Pasteur Institute of Iran, and all methods were performed in accordance with the relevant guidelines and regulations.
The study was carried out in compliance with the ARRIVE guidelines. In this study, HUVEC, L929, and SW1353 cell lines also isolated Adipose-derived stem cells (ADSCs) and chondrocytes from 6-month-old male New Zealand white rabbits were used. Stem cells and chondrocytes were isolated from sacrificed animals in other studies according to the protocols established at the National Cell Bank of Iran [2,26]. In short, anesthesia was induced by injecting ketamine (35 mg/kg) and xylazine (8 mg/kg) intramuscularly. Then to harvest samples, barbiturate (100 mg/kg) was injected intraperitoneally. Harvested samples of Hyaline cartilage were washed multiple times with cell culture medium, sliced, and added to the trypsin-EDTA solution (0.25 %, Sigma, USA) and placed in the incubator (37°C). After 30 min, the samples were digested overnight in collagenase type II solution (0.08 mg/ml, Sigma, USA) in the incubator (37°C and 5% CO2). The chondrocytes have the spherical morphology of mature cells a short time after isolation, but they de-differentiate and gain a spindle-shaped morphology after cultivation in a cell culture plate and more extended incubation (~ 14 days); so we used freshly isolated chondrocytes in this study [2].

For ADSCs isolation, the adipose tissue was collected from the rabbit interscapular region. First, it was put in the DMEM cell culture medium containing antibiotic/antimycotic solution (1%, Invitrogen, USA). After separation of connective tissues, blood vessels, and fragmentation, the fragments were washed with PBS solution containing antibiotic/antimycotic (1%, Invitrogen, USA). Afterwards, they were added to collagenase type I (0.02 mg/ml, Sigma, USA) and were kept for 1 hour in the incubator at 37°C. The cells were then centrifuged, washed, and transferred to the culture medium containing Dulbecco's Modified Eagle's Medium (DMEM, GIBCO, Scotland)/Ham's F12 supplemented with 100 µg/ml streptomycin, 100 U/ml penicillin (Sigma, USA), and 10% fetal bovine serum (FBS, Seromed, Germany).

According to our previously published report [62], ADSCs' multi-potency was assessed in vitro for adipogenesis, osteogenesis, and chondrogenesis.

2.3.2 Microfluidic device fabrication

Basic photolithography accompanied by deep reactive-ion etching (DRIE) of silicon using an oxide mask was used for the master fabrication process. Afterwards, using soft lithography, the pattern was transferred to PDMS (Sylgard 184 Silicon Elastomer Kit, Dow Corning) with the 10:1 weight ratio of the base polymer to the curing agent according to the previously published report [63].

2.3.3 Cell-imprinted-based integrated microfluidic device fabrication

First, a cell-imprinted substrate was prepared using a microfluidic chip. For this purpose, after sterilization by treatment in the autoclave, a microfluidic chip with channels side facing down was placed on a cell culture plate. The solution with the concentration of 6×10^6 of template cells in 150 µl of culture medium was prepared and injected into the chip using a syringe pump with a flow rate of 50 µl/min. The cell injection was continued until all the microchannels were filled with the cells and gained the desired pattern. In order to ensure the filling of microchannels, the microfluidic chip was observed under a microscope during the injection.

The set was put inside the incubator for 7 hours to enable the cells to adhere to the cell culture plate's surface while obtaining the microfluidic chip pattern. After removing the microfluidic chip from the cell culture plate, the plate's surface, which had the pattern of template cells, was washed with PBS. Then the adhered template cells were fixed by 4% glutaraldehyde solution for 1 hour. After washing the fixed template cells with distilled water and, after drying, PDMS casting was done. In order to transfer the cell pattern to the PDMS curing process was carried out at 37°C for 1 day. After completing the curing process, the silicone layer was peeled off from the cell culture plate. The cell-imprinted substrate was then washed with 1 M NaOH solution to remove the residues.

For the fabrication of a cell-imprinted-based integrated microfluidic device, a new microfluidic chip should be aligned on the cell-imprinted substrate and attached to it using argon plasma. As the microfluidic chip's design is in parallel lines, and the cell-imprinted substrate pattern is the same as the microfluidic chip pattern, they can easily align under the microscope after argon plasma treatment. Then in order to ensure the bonding of the upper microfluidic chip and the bottom cell-imprinted substrate, the cell-imprinted-based integrated microfluidic device was placed on the 80 ºC hot plate for 1 hour. This cell-imprinted-based integrated microfluidic device can be used for future cell culture for biomedical applications such as drug analysis on template cells or stem cell differentiation to template cells. After removing cells with trypsin injection, washing and sterilization, the cell-imprinted-based integrated microfluidic device can be used again.

2.3.4 Application of the cell-imprinted-based integrated microfluidic device in stem cell differentiation

A cell-imprinted-based integrated microfluidic device was fabricated based on chondrocyte as template cell according to the above procedure. It was then sterilized using autoclave treatment. There is a static and a dynamic stage for differentiation of ADSCs in the cell-imprinted-based integrated microfluidic device. In the static stage, the solution with the concentration of 3×10^6 of ADSCs in 150 µl of culture medium was prepared and injected into the integrated microfluidic device using a syringe pump with a flow rate of 50 µl/min until the cells filled all the microchannels. In order to allow the attachment of cells

to the surface of the cell-imprinted substrate, the integrated microfluidic device should be placed inside the incubator for 4 hours.

A parallel network of 4 cell-imprinted-based integrated microfluidic devices was used to have more differentiated ADSCs to chondrocytes simultaneously. This network was connected to a 25 ml syringe full of cell culture medium. In a dynamic stage during 14 days of ADCSs differentiation to supply the cell culture medium dynamically, a syringe pump with a flow rate of 1 ml/day was connected to the network mentioned above, and this set was placed in the incubator for 14 days. There is no need to change the cell culture medium by an operator like traditional cell culture by this method.

Trypsin-EDTA treatment was done using an insulin syringe instead of pippets in the traditional digestion methods in cell culture plates to remove differentiated cells from inside the cell-imprinted-based integrated microfluidic device after 14 days.

2.3.5 Microscopy observations

Scanning electron microscopy (SEM) was used to characterize the cell-imprinted substrate and observe its structure and morphology.

For fluorescence microscopy, the upper microfluidic chip was not bonded to the bottom cell-imprinted substrate for better and easier imaging. So, after ADSCs culture on a cell-imprinted substrate in a microfluidic chip, the microfluidic chip can be removed. For this purpose, to prevent leakage, two rigid plexiglass sheets were used to compress the upper microfluidic chip and the bottom cell-imprinted substrate, which were aligned under a microscope. Cultured cells on the cell imprinted substrate were then fixed for 20 minutes in paraformaldehyde (4%, Sigma, USA) before staining. Antibodies employed for staining are shown in Table 1.

Table 1
Employed antibodies for staining

Product type	Description
Phalloidin, FITC conjugated	Staining of the actin filaments
Fluorescent AlexaFluor488 labeled wheat germ agglutinin (WGA)	Cell membrane visualization
Primary Antibody	Rabbit Polyclonal Antibody Collagen II (LSC354627)
Secondary Antibody	Goat Anti-Rabbit IgG H&L (FITC) (ab6717)

After five days of ADSCs culturing on the cell-imprinted substrate, FITC conjugated phalloidin (Sigma, USA) was used for the actin filaments staining; also, samples were stained with fluorescent AlexaFluor488 labeled wheat germ agglutinin (WGAAlexaFluor488, Invitrogen, USA).

After 14 days of chondrogenic differentiation of cultured ADSCs on a cell-imprinted substrate, Alcian blue staining was done to evaluate the proteoglycan expression. A solution of 2.5 % glutaraldehyde (diluted from 50 % solution; Merck) was prepared in25 mM sodium acetate and 0.4 M $MgCl_{2,}$ and to have 0.05 % concentration, Alcian blue 8GX (Sigma, Germany) dissolved in the prepared solution. After Alcian blue staining, the samples were washed with a 3% acetic acid solution [64].

In addition, after 14 days of chondrogenic differentiation of cultured ADSCs on a cell-imprinted substrate, immunofluorescence staining of collagen type II was done [26,39]. The samples were washed with ice-cold PBS two times and incubated for 10 minutes in 0.25 % Triton X-100 to permeabilize the cell membrane. Then, they were washed with PBS three times for 5 min each. Afterwards, they were incubated with 1% BSA for 30 minutes to block the secondary antibody reaction as the additional background color and subsequently incubated with the primary antibody (1: 100 dilution with PBS) for 1 hour at room temperature, followed by washing with PBS three times for 5 min each. Cells were then incubated in the dark with secondary antibody (1:150 dilution with PBS) for 1 hour at room temperature, followed by washing three times for 5 min each in the dark. After four washes in the dark, DAPI (Invitrogen, USA) was added and removed immediately. Then PBS was poured onto the samples, and they were evaluated using a fluorescent microscope (Labomed tcs400).

2.3.6 Gene expression analysis

In order to determine the expression of Aggrecan, Collagen I, Collagen II, and Sox9 genes, the Real-time PCR assay by StepOne instrument was used (Applied Biosystems, USA), and to design forward and reverse primers, the sequences of target genes were obtained from the NCBI database (Table 2). In this study, undifferentiated (normal) ADSCs and differentiated ADSCs (on the traditional cell-imprinted substrate and in a cell-imprinted-based integrated microfluidic device) were considered as control and test groups, respectively.

According to the manufacturer's instruction, a blood/Cultured cell total RNA mini kit (Yekta Tajhiz Azma, Iran) was used for total RNA isolation from samples after 14 days. Recombinant DNase I (TaKaRa, Japan) was used for removing Genomic DNA. Then the PrimeScript RT Reagent Kit (TaKaRa, Japan) was used for reverse transcription of total RNAs to produce single-strand cDNA. Finally, SYBR Premix Ex Taq II (Takara, Japan) was used for the Real-time PCR analysis with GAPDH as an endogenous control. The comparative Ct method was used for analyzing each gene expression quantitatively. Each target gene Ct value was normalized to their respected GAPDH.

Table 2

Primers sequences used in Real-time PCR [a]

Name of the corresponding protein	Sequence (5' ◊3')		Length (bp)
GAPDH	Fw	5'-GGCACAGTCAAGGCAGAGAAC-3'	115
	Re	5'-CCACATACTCAGCACCAGCATC-3'	
Aggrecan	Fw	5'-CACCACGCCTTCTGCTTCC-3'	105
	Re	5'-TGTCACCATCCACTCCTCCAC-3'	
Collagen I	Fw	5'-GTCCTTCTGGTCCTCGTGGTC-3'	159
	Re	5'-CTTCGCCATCATCTCCGTTC-3'	
Collagen II	Fw	5'-GGAGCAGCAAGAGCAAGGAC-3'	151
	Re	5'-TGAGAGCCCTCGGTGGAC-3'	
Sox9	Fw	5'-GCTGGACTGGGAGTTGGAGAG-3'	179
	Re	5'-AAGGCGAATTGGAGAGGAGG-3'	

[a] Abbreviations: Fw, forward; Re, reverse.

3. Results

3.1 Computational fluid dynamics analysis

As it was mentioned in Sect. 2.2, after mesh convergence study and a proper mesh selection, simulation of the chip with 40 μm microchannels with the inlet injection velocity of 0.012291 m/s and the concentration of 2×10^6 cells in 170 microliters cell culture medium was performed. As not all cells are the same size, a normal distribution of cell size with an average diameter of 12 μm (almost the same as SW1353 cell line) was considered in this simulation.

Figure 2.a shows the velocity profile in the microfluidic chip with 40 μm microchannels, and Fig. 2.b shows the velocity profile around terminal microposts. As can be seen in the microfluidic chip, we have laminar flow. Around the terminal microposts, where the available space for fluid passage decreases, the velocity increases, and maximum velocity occurs in these 2 μm free spaces between the chip and microposts walls.

When high shear stress exists, the rupture of a cell membrane occurs, and this phenomenon is called cell disruption. It is the principal physical cause of the death of cells. Born et al. studied the damage to suspended cells due to shear stress and reported the shear stress range of 200–700 Pa for cell disruption in laminar flow. Figure 2.c shows the shear stress profile in the microfluidic chip with 40 μm microchannels and around terminal microposts. Figure 2.d shows the pressure contour around terminal

microposts. As shown in the microfluidic chip, the shear stress applied to the cells is almost the same along the microchannels. Around the terminal microposts, where the available space for fluid passage decreases, the shear stress increases, and maximum shear stress occurs in these 2 μm free spaces between the chip and microposts walls. The surface average shear stress in the microfluidic chip is 0.1504 Pa. This number is below the physiological shear stress of 1 Pa experienced by vascular endothelial cells [65].

As mentioned, when the cell-imprinted substrate is made, the cells are injected into the chip in a relatively short time. Then the chip is separated from the syringe pump and placed inside the incubator. For stem cell differentiation application of the cell-imprinted-based integrated microfluidic device, the stem cells are injected into the integrated microfluidic device and differentiate into chondrocytes in the incubator during the dynamics injection of the culture medium using a syringe pump for about 14 days. So, at this stage, the stress applied to the cells inside the microfluidic chip should be consistent with the in vivo conditions. Therefore, fluid flow simulations were performed for lower flow rates of the culture medium in the dynamic stage. For a flow rate of 250 μl/day of culture medium per chip, the surface average shear stress in the microfluidic chip was $7.34 * 10^{-4}$ Pa. In previous experiments, the interstitial fluid level in the intra-articular cartilage surface and various articular surface layers was in the range of 10^{-5} to 10^{-2} dyne/cm^2. So, the average shear stress of $7.34 * 10^{-3}$ dyne/cm^2 that is the shear stress applied in this work, is consistent with the cartilage space's interstitial fluid level.

Figure 3.a shows the cell trajectories throughout the microfluidic chip when the first cells reach the terminal microposts. The color of the cells indicates their velocity (m/s) in the chip. As can be seen, the particles' velocity is approximately the same along all 40 μm microchannels. With the help of simulation, the time when the first cells reach the end of the microchannels can be obtained. As shown in Fig. 3.a, since the microfluidic chip design is symmetrical about the x-axis, the particle distribution on the chip surface is also symmetrical. The movement of cells in the top, bottom, and two central microchannels is behind the other microchannels, and these microchannels are the last microchannels to be filled. The movement of cells in the microfluidic chip can be obtained as animation using simulation and can be used as a guide before laboratory experiments (Supplementary video 1). This video can also be compared and validated by experimental injection of cells in the laboratory. Figure 3.b shows the histogram of particle distribution throughout the microfluidic chip when the first cells reach the terminal microposts. As can be seen, almost all microchannels have received a similar distribution of cells, and the number of cells in the inlet sections, which are larger, is higher than the 40 μm microchannels. Also, the number of cells decreases along the microfluidic chip from the inlet towards the outlet.

Next, we investigated the effect of cells' injection flow rate (input velocity in simulation). Figure 3.c shows the velocity changes along the centerline of the input channel for different inlet velocities in the microfluidic chip with 40 μm microchannels. As can be seen, the velocity slightly increases, reaches a constant value, and decreases again after reaching the flow's partition in the next channels. Figure 3.d shows velocity changes along a cut line on the centerline (before reaching the central channel's terminal microposts) for different inlet velocities. Also, Fig. 3.e shows velocity changes in the vertical direction of a

microfluidic chip in eight consecutive microchannels for different inlet velocities. As can be seen, all eight microchannels have the same velocity profile, and this is true for all microchannels; and according to Fig. 3.d, the velocity remains constant along microchannels. So, according to Fig. 3.d and Fig. 3.e, it can be concluded that all microchannels of the chip have almost the same velocity profile. Figure 3.f shows velocity changes in the direction of a 2 μm vertical free distance between the micropost and the microchannel wall for different inlet velocities. As can be seen in this area, the amount of velocity is higher than other areas, and it is in parabolic shape because, in contact with the walls, the velocity is zero, but in the distance between the micropost and the microchannel wall, the velocity increased by a reduction in available passage space.

Figure 3.g shows the shear stress changes along a diagonal cut line from the central microchannel's bottom-left point to its top-right point (before reaching the central microchannel's terminal microposts) for different inlet velocities in the microfluidic chip with 40 μm microchannels. As can be seen, the shear stress is higher near the walls and tends to almost zero as it approaches the microchannel's midpoint. Also, the higher the input velocity, the higher the shear stress applied to the cells. Figure 3.h shows shear stress changes along the 2 μm vertical free distance between the micropost and the microchannel wall for different inlet velocities. Shear stress increases near the micropost and microchannel wall. Figure 3.i shows a histogram of cells' position along the microfluidic chip at different inlet velocities. As the changes in input velocity also change cells release time and the time it takes for the first cells to reach the end of the channels, in a similar time index, the change in velocity does not affect the location and number of cells per location much. The point to be noted is that although the shear stress applied to the cells decreases as the inlet velocity decreases, the microchannels' time to fill increases. This means that cells are out of the incubator for a longer time, and the possibility of the settling of the cells inside the syringe increases, which will cause an error in the experimental results.

In addition, to study the effect of input velocity changes, similar to the above simulations, which were performed for cells with an average diameter of 12 μm in normal size distribution (Fig. 4.a), other simulations were performed for cells with different diameters. Thus, the inlet velocity and the number of cells in 170 μl cell culture medium were fixed at 0.012291 m/s and 2×10^6 respectively, but the cell diameter and cell size distribution were almost similar to freshly isolated chondrocytes, L9292 and HUVEC cell lines (average diameters of 8, 14 and 19 μm respectively). The particle size distribution profiles intended for these cells are shown in Fig. 4.a. As can be seen, a wider particle size distribution is considered for larger cells according to laboratory observations.

Fig. 4.b and Fig. 4.c show cell trajectories in the microfluidic chip with 40 μm microchannels for two different average diameters of 8 μm and 19 μm. As can be seen, for the same concentration of 2×10^6 cells in 170 μl cell culture medium and the same time index, the number of cells with 8 μm diameter is not enough to fill the microfluidic chip with 40 μm microchannels, so for smaller cells, the chip with smaller microchannels, more of these cells in a constant volume of cell culture medium (which increase the injected cells concentration) should be used.

Next, the velocity (0.012291 m/s) and the diameter of the cells (12 µm) were considered constant as the initial simulation, but the effect of increasing the number of injected cells in 170 µl volume of cell culture medium (increasing injected cells concentration) was investigated. Figure 4.d shows the histogram of the cell's position along the microfluidic chip with different numbers of cells in the constant volume of the injected culture medium. As can be seen, as the input cell concentration increases, the number of cells increases at the same spatial distance, resulting in a more orderly cell pattern. Figure 4.e and Fig. 4.f also show cell trajectories in the microfluidic chip with 40 µm microchannels for two different cells number in a constant volume of cell culture medium when the first cells reach the terminal microposts. As it can be seen, higher cell concentration leads to more cell-loaded microchannels.

All the above simulations were performed for microfluidic chips with 25 µm microchannels. Similar results were obtained for changes routine in terms of input velocity, diameter, and the number of cells. It is noteworthy that for cells with the same diameter, same cell number per unit volume, and the same injection flow rate of the syringe pump, the effect of reducing the width of the microchannel was on the values of velocity, shear stress, and the number of cells and time required to fill the microchannels (FigS2).

Tables 3 and 4 show a comparison of the surface average and the surface maximum along the microfluidic chip with 40 µm and 25 µm microchannels for shear stress and velocity. The rows are for the same injection flow rate of the syringe pump in both chips. Comparing the shear stress and velocity results for two chips with different microchannel diameters but with the same cell injection conditions shows that the surface maximum values for both chips are approximately the same but increase for the surface average of the chip with smaller microchannels. Also, since the channels are smaller, the number of cells along the chip length will be less in almost identical locations (compare Fig. 3.b and FigS2.f).

Table 3
Surface average of shear stress and velocity for two microfluidic chips with 40 µm and 25 µm microchannels

Surface Average					
40 µm			25 µm		
v_inlet (m/s)	Shear stress (Pa)	Velocity magnitude (m/s)	v_inlet (m/s)	Shear stress (Pa)	Velocity magnitude (m/s)
0.001536	0.018811	4.91E-04	0.002458	0.049106	7.27E-04
0.003073	0.037625	9.82E-04	0.004916	0.098211	0.0014538
0.006145	0.075238	0.001963	0.009833	0.19644	0.0029079
0.012291	0.15049	0.0039264	0.019666	0.39288	0.0058158
0.024582	0.30098	0.0078528	0.039331	0.78575	0.011631
0.04097	0.50163	0.013088	0.065552	1.3096	0.019386

Table 4
Surface maximum of shear stress and velocity for two microfluidic chips with 40 µm and 25 µm microchannels

Surface Maximum					
40 µm			25 µm		
v_inlet (m/s)	Shear stress (Pa)	Velocity magnitude (m/s)	v_inlet (m/s)	Shear stress (Pa)	Velocity magnitude (m/s)
0.001536	11.579	0.0042421	0.002458	11.59	0.0041847
0.003073	23.159	0.0084848	0.004916	23.181	0.0083694
0.006145	46.31	0.016967	0.009833	46.367	0.01674
0.012291	92.628	0.033936	0.019666	92.733	0.033481
0.024582	185.26	0.067873	0.039331	185.46	0.06696
0.04097	308.76	0.11312	0.065552	309.1	0.1116

Therefore, considering the application of future cell culture in the cell-imprinted-based integrated microfluidic device, more differentiated stem cells are needed to place on scaffolds and transplant in the animal's body; it is better to use a microfluidic chip with 40 µm microchannels, which has a higher capacity. Another point to note is that it takes less time for the first cells to reach the terminal microposts in a chip with smaller microchannels, and it should be noted that this short injection time is more difficult to control, and prolonging the injection time causes excessive cell accumulation. It affects their adhesion and may push cells out of the microchannels' outlet by applying more pressure.

In this part, by simulation, the parameters which affect the experiment were investigated. Therefore, for cell-imprinted substrate preparation, in addition to selecting the appropriate inlet velocity for that does not exert too much shear stress on the cells and does not allow the cells to be out of the incubator for a long time during injection so as not to damage the cells and cause the cells to settle inside the insulin syringe, the sufficient concentration of injected cells should be selected so that we can have a regular pattern of cells in parallel lines. Also, the injection flow rate of the dynamic stage cell culture medium can be selected so that applied shear stress in the integrated microfluidic device is consistent with the cartilage space's interstitial fluid level. Simulation helps us get an overview of experimental conditions before entering the lab without wasting materials and time.

3.2 Validation of numerical analysis with experimental analysis

The SW1353 cell line with an average diameter of 12 µm and a concentration of 1380000 cells in 170 µl cell culture medium in a microfluidic chip with 40 µm microchannels and a syringe pump flow rate of

2.12 ml/h were used to validate the simulation results. For this purpose, after preparing the cell injection conditions using a light microscope and a camera, a video of the movement of cells within fluid flow at a frame rate of 30 frames per second was recorded. To validate the simulation, we applied exactly the same conditions in the simulation and prepared an animation of the cell trajectories at the same frame rate. The position of the chip under the microscope was tried to be exactly the same as the part of the chip in the simulation from which the animation was prepared. Then both videos were put beside each other for comparison (Supplementary video 2).

Comparing simulation and experimental videos, we concluded that the simulation accurately predicted the movement of cells in the microfluidic chip and that the cell movements differed in velocity in a few hundredths of a second. This slight difference in simulation and experimental results may be due to the following:

1. When making a microfluidic chip, after several times of molding and removing the PDMS layer from the silicon wafer, some of the microposts may not form properly. They may remain inside the silicon wafer, causing some microchannels to miss some of their terminal microposts. So the resistance against the fluid flow and passing cells in some microchannels may be decreased. Compared with the ideal simulation of the same microchannels, this can cause some differences in experimental.

2. In experimental, cell mixing (by pipette up/down) may not be performed well, and the cell concentration inside the insulin syringe may not be uniform, and some cells may make aggregates.

3. There might be an error in cell counting, and the cell number might differ from what was counted by the hemocytometer slide and trypan blue staining (human error).

4. The syringe pump's flow rate used to inject the cell into the microfluidic chip in the laboratory may not be exactly the set value.

Despite the above reasons, the simulation results agree with the experimental results, which shows the power of computational methods that in a virtual laboratory, suitable conditions for experimental studies can be obtained without wasting time and money in a real laboratory.

3.3 Microscopy observations

Figure 5.a shows the schematic of the cell-imprinted-based integrated microfluidic device fabrication procedure. Before experimenting with chondrocytes as the main cells in this study, which needs to be isolated from the rabbit's cartilage, the microfluidic chip's functionality in trapping cells and creating a regular pattern the same as the microfluidic chip geometry was evaluated for HUVEC and L929 cell lines.

Figure 5.b shows 40μm microchannels of the microfluidic chip after injecting the HUVEC cell line with a syringe pump. The microchannels were almost filled with cells in regular controlled places, and this pattern transferred to the cell-culture plate and looks like regular paving (Fig. 5.c). Figure 5.d also shows the same results for the L929 cell line in 25μm microchannels of the microfluidic chip after injection and

their regular pattern transferred to the cell-culture plate (Fig. 5.e). As it was mentioned, it was proved that instead of cell culture in conventional rigid polystyrene plates, cell-imprinted substrates based on their topography provide conditions similar to those of cells' natural growth environment, but in traditional imprinting methods, the placement of cells was random, and the probability of the cells to place exactly on the cell-imprinted topography was low.

In this study, by applying a microfluidic chip, the topography of template cells regularly transfers to the cell culture plate. So, a regular cell-imprinted substrate can be made after mold casting on these regular cellular topographies by PDMS. These regular cell-imprinted substrates can provide platforms for anti-cancer drug analysis in future studies by culturing the same cell line as the template cell line that has been used for cell imprinting.

After evaluating our microfluidic chip's functionality with test cells (HUVEC and L929 cell lines), experiments were performed with chondrocytes, and they were injected into the microfluidic chip with 40μm microchannels. Figure 6.a shows the microchannels were almost filled with chondrocytes in regular controlled places and this pattern transferred to the cell-culture plate (Fig. 6.b).

The SEM image of one line of the regular chondrocytes' pattern on the cell-imprinted substrate is shown in Fig. 6.c. As can be seen, chondrocytes' topography in a regular arrangement similar to the microfluidic chip's parallel microchannels was transferred to the PDMS replica by mold casting.

Also, proteoglycan's presence secreted by differentiated ADSCs on the cell-imprinted substrate surface in the microfluidic chip was confirmed by Alcian blue staining (Fig. 6.d).

Phalloidin staining, WGA staining, and optical microscopy of ADSCs cultured for five days on a chondrocyte-imprinted substrate in a microfluidic chip are shown in Fig. 6.e-g, respectively. As it can be seen, just after five days, the spindle morphology of ADSCs was almost converted into chondrocyte's spherical morphology. Also, ADSCs created a regular pattern like that of the microfluidic chip on parallel lines in the predicted locations on the regular cell-imprinted substrate.

As it was mentioned, uncertainty over whether ADSCs have been specifically positioned on the chondrocyte pattern on the cell-imprinted substrate is the key issue with the traditional imprinting methods. The location of the cells is completely unpredictable. In this study, based on the parallel lines in microfluidic chip design, a similar chondrocyte pattern is formed on the cell–imprinted substrate. In the cell-imprinted-based integrated microfluidic device fabrication procedure, before the bonding stage, the upper microfluidic chip and the chondrocyte-imprinted substrate can be easily aligned on their similar lines. This approach is objective, controlled, and non-random, unlike previous imprinting techniques. ADSCs' pathway is predicted in the cell-printed-based integrated microfluidic device to be precisely positioned on the chondrocyte-imprinted pattern. After 14 days of differentiation, ADSCs will get the chondrocyte phenotype.

In addition, after 14 days, ADSCs cultured on the cell-imprinted substrate were stained with collagen II antibody, and cell nuclei were stained with DAPI (Fig. 7.a). Also, evaluation of chondrogenic differentiation in 3 samples according to image processing with IMAGE J software showed collagen II (chondrocyte specific gene marker) relative expression of about 68%.

3.4 Gene expression analysis

The gene expression analysis of the cultured ADSCs in the cell-imprinted-based integrated microfluidic device was compared with cultured ADSCs on the traditional cell-imprinted substrate (Fig. 7.b.). Undifferentiated ADSCs which were grown on standard cell culture flasks were considered as control. In ADSCs cultured in the cell-imprinted-based integrated microfluidic device compared with cultured ADSCs on the traditional cell-imprinted substrate, collagen II expression (a chondrocyte specific gene marker) is up-regulated while the expression of collagen I is significantly down-regulated.

As a criterion for comparison between chondrogenic differentiations in different methods, the ratio of collagen type II to collagen type I expressions was evaluated for cultured ADSCs in the cell-imprinted-based integrated microfluidic device and on the traditional cell-imprinted substrate. According to Fig. 7.b, this ratio is significantly higher for differentiation of ADSCs in the cell-imprinted-based integrated microfluidic device (3.39/0.137 ~ 24.7) compared to the traditional cell-imprinted substrate (7.23/0.68 ~ 10.6).

4. Discussion

Cell-imprinting technology is an innovative technique for directing stem cell fate by molding substrates from target cells. This method's functionality has been proven in previous research for various cells for different applications such as drug analysis and stem cell differentiation [2,24–30,66]. In this method, the template cells are cultured and fixed on the cell culture plate's surface. Then by polydimethylsiloxane (PDMS, Sylgard 184) mold casting, the template cell cellular plasma membranes and nucleus topography is transferred to the cured PDMS layer, which can be used as a new cell-imprinted substrate for future cell culture.

The major issue with the conventional imprinting method is its poor efficacy because the cells' location is random. Hence, the likelihood of the secondary cell being placed on the template's cell-imprinted substrate is low. If a cell finds a pattern by chance, it would probably go inside the hole to form a new shape, but this is not a reproducible result, and there is no power to regulate cells' migration into patterns according to previous experiments. The second weakness of previous cell culture approaches on a PDMS cell-imprinted substrate is synonymous with failures when a bubble is formed under the PDMS substrate. This PDMS substrate may be submerged in the culture medium, and the cells on the substrate of PDMS would remain without the medium. Also, there is the possibility of cells migrating from the PDMS substrate to the polystyrene culture plate, which can cause cell culture errors.

In this study, in order to eliminate the drawbacks of traditional imprinting methods, the placement of template cells was predicted by using a microfluidic chip, and imprinted cells got the same pattern as the parallel line of the microfluidic chip. In order to increase the efficiency of traditional imprinting methods using another microfluidic chip aligned on the cell-imprinted substrate, the culture of the secondary cells, which can be the same as template cell (while preserving normal cell activity) or stem cell (to be differentiated to the template cell) based on the biomedical application, is non-random and targeted. Also, the probability of secondary cells placement on the cell-imprinted substrate was increased. In addition, cell culture in this cell-imprinted-based integrated microfluidic device was dynamic using a syringe pump, and the culture medium passed continuously over the cells. In contrast with conventional cell culture methods, there was no need to change the cell culture medium and daily care by an operator, which increases the risk of error. Also, in the case of stem cell differentiation, a network of these cell-imprinted-based integrated microfluidic devices was connected to a syringe pump. It simultaneously supplied more differentiated ADSCs to chondrocytes without any chemical growth factors and only with a physical signal and improved stem cell differentiation efficiency, increasing the success of future cell transplantation procedures. This study's cell-imprinted-based integrated microfluidic device can be washed after removing cells by trypsin-EDTA treatment and autoclaved again for further use. All of the above advantages led to a significant reduction of the final cost.

Phalloidin, WGA, and Alcian blue staining results showed that the spindle morphology of ADSCs cultured in the microfluidic device on the cell-imprinted substrate was converted into spherical morphology of chondrocyte by placement into the chondrocyte-imprinted topography. Collagen II and Alcian blue staining as a criterion of chondrogenic differentiation showed positive results. The gene expression analysis showed that ADSCs differentiation in the cell-imprinted-based integrated microfluidic device was successful by increasing collagen II expression and decreasing collagen I expression than control, which was the undifferentiated ADSCs cultured on a cell culture flask. Compared to traditional imprinting, ADSCs differentiation was improved because the ratio of collagen II to collagen I expressions was 2.3 times higher for ADSCs differentiation in the cell-imprinted-based integrated microfluidic device than traditional cell-imprinting methods.

Previous experiments have shown that all cells with possible chondrogenic differentiation capability can be differentiated into chondrocytes on the traditional chondrocyte-printed substrate [26]. So in our chondrocyte-imprinted-based integrated microfluidic device, too, all cells with potential chondrogenic differentiation can be differentiated into chondrocytes.

This method, which is safe, cheap, reproducible, and well-controlled, can be used for all applications involving cell culture instead of cell culture plates in the laboratory or clinic. It can also be generalized to other adherent template cells or other cell transplantation methods, such as heart, skin, neuron, bone, etc. According to the final application, the template cell can be isolated from the tissue or chosen from cell lines.

5. Conclusion

In this study, a cell-imprinted-based integrated microfluidic device was presented for biomedical applications, which improved the traditional imprinting cell-imprinted substrate efficiency by controlling the cell culture space. In this method, template cells were prepared in a regular pattern employing a microfluidic chip. After mold casting by PDMS, it was used as a cell-imprinted substrate under another microfluidic chip with the same pattern. When secondary cells were injected into the cell-imprinted-based integrated microfluidic device, there were only template cell patterns under them where they could be placed on it. In addition to PDMS, any materials with nanometer and micrometer dimensions can execute the process of making a cell-imprinted-based integrated microfluidic device based on the cell membrane topography.

In our method, cell culture was objective, non-random, and dynamic in contrast with traditional imprinting methods. Also, the cell culture medium continuously passed through cells.

Also, by applying microfluidic devices and reducing the experimental device's size to micrometer levels, the amount of cell culture medium and the number of cells required in an experiment was reduced leads to a more economical process.

In the stem cell differentiation application, it was possible to supply more differentiated stem cells using a network of multiple integrated microfluidic devices connected to a syringe pump, which can be useful for future clinical trials.

In comparison with rigid polystyrene cell culture plates, as the topography of the cell-imprinted substrate is consistent with the target cells' natural phenotype, the cells' function is much closer to their normal behavior in the body. So, this cheap and reproducible procedure can be used in all cell culture applications, such as growth and proliferation (while preserving normal cell activity) for drug analysis applications or differentiation for various tissue engineering and cell therapeutic applications.

Numerical simulation results can also be used as a guide to determine the effective factors in experimental conditions before entering the laboratory. The simulation results in this study showed that parameters such as injection speed, number, and size of cells, as well as channel dimensions, are effective in the experimental results, and suitable conditions were obtained using simulation before experimental analysis. Validation of simulation results with experimental results showed the power of numerical methods, which saves time and money. In fact, without attending the laboratory, we designed a virtual lab that does not require cell culture materials, the preparation of cell lines, the isolation of cells from the animals, and the operator for culturing, passage, and daily care of cells.

Declarations

Declaration of competing interests

There are no conflicts to declare.

Acknowledgments

This work was supported by Iran National Science Foundation (INSF) [grant no. 96016453].

Author Contributions

S.Y.K: Performed the whole research and wrote the article. M.K.M: Designed the research and edited the article. S.B: Developed the idea, supervised the whole project, and edited the article.

References

1. Scadden, D. T. The stem-cell niche as an entity of action. *Nature.* **441**, 1075–1079 (2006).
2. Mahmoudi, M. *et al.* Cell-imprinted substrates direct the fate of stem cells. *ACS Nano.* **7**, 8379–8384 (2013).
3. Li, W., Yan, Z., Ren, J. & Qu, X. Manipulating cell fate: dynamic control of cell behaviors on functional platforms. *Chem. Soc. Rev.* **47**, 8639–8684 (2018).
4. Bonakdar, S. *et al.* Preparation and characterization of polyvinyl alcohol hydrogels crosslinked by biodegradable polyurethane for tissue engineering of cartilage. *Mater. Sci. Eng. C.* **30**, 636–643 (2010).
5. Place, E. S., Evans, N. D. & Stevens, M. M. Complexity in biomaterials for tissue engineering. *Nat. Mater.* **8**, 457–470 (2009).
6. Löfberg, J. & Ebendal, T. Substrate topography and shape of motile cells. *Experientia.* **36**, 508–510 (1980).
7. Engler, A. J., Sen, S., Sweeney, H. L. & Discher, D. E. *Matrix Elasticity Directs Stem Cell Lineage Specification. Cell.* **126**, 677–689 (2006).
8. Pelham, R. J. & Wang, Y. L. Cell locomotion and focal adhesions are regulated by substrate flexibility. Proc. Natl. Acad. Sci. U. S. A. 94, 13661–13665(1997).
9. Lo, C. M., Wang, H. B., Dembo, M. & Wang, Y. L. Cell movement is guided by the rigidity of the substrate. *Biophys. J.* **79**, 144–152 (2000).
10. Stroka, K. M. & Aranda-Espinoza, H. A biophysical view of the interplay between mechanical forces and signaling pathways during transendothelial cell migration. *FEBS J.* **277**, 1145–1158 (2010).
11. Ali, M. & Shear, J. B. Real time remodeling of cellular morphology using optical imprinting of cell-culture substrates. *Biomed. Phys. Eng. Express.* **5**, 035029 (2019).
12. Guilak, F. *et al.* Control of Stem Cell Fate by Physical Interactions with the Extracellular Matrix. *Cell Stem Cell.* **5**, 17–26 (2009).
13. Choi, Y. Y. *et al.* Controlled-size embryoid body formation in concave microwell arrays. *Biomaterials.* **31**, 4296–4303 (2010).
14. Hosseini, V. *et al.* Engineered contractile skeletal muscle tissue on a microgrooved methacrylated gelatin substrate. *Tissue Eng. - Part A.* **18**, 2453–2465 (2012).

15. Unadkat, H. V. *et al.* An algorithm-based topographical biomaterials library to instruct cell fate. Proc. Natl. Acad. Sci. U. S. A. 108, 16565–16570(2011).
16. Markert, L. D. A. *et al.* Identification of distinct topographical surface microstructures favoring either undifferentiated expansion or differentiation of murine embryonic stem cells. *Stem Cells Dev.* **18**, 1331–1342 (2009).
17. Bucaro, M. A., Vasquez, Y., Hatton, B. D. & Aizenberg, J. Fine-tuning the degree of stem cell polarization and alignment on ordered arrays of high-aspect-ratio nanopillars. *ACS Nano.* **6**, 6222–6230 (2012).
18. Kumari, S. *et al.* Shaping Cell Fate: Influence of Topographical Substratum Properties on Embryonic Stem Cells. *Tissue Eng. - Part B Rev.* **24**, 255–266 (2018).
19. Hernandez, D. S., Ritschdorff, E. T., Connell, J. L. & Shear, J. B. In Situ Imprinting of Topographic Landscapes at the Cell-Substrate Interface. *J. Am. Chem. Soc.* **140**, 14064–14068 (2018).
20. Schmidt, S., Lilienkampf, A. & Bradley, M. New substrates for stem cell control. *Philos. Trans. R. Soc. B Biol. Sci.* **373**, 0–1 (2018).
21. Yang, L., Ge, L. & van Rijn, P. Synergistic Effect of Cell-Derived Extracellular Matrices and Topography on Osteogenesis of Mesenchymal Stem Cells. *ACS Appl. Mater. Interfaces.* **12**, 25591–25603 (2020).
22. Wang, W. *et al.* Efficient Capture of Cancer Cells by Their Replicated Surfaces Reveals Multiscale Topographic Interactions Coupled with Molecular Recognition. *ACS Appl. Mater. Interfaces.* **9**, 10537–10543 (2017).
23. Zhou, X. *et al.* Reversed cell imprinting, AFM imaging and adhesion analyses of cells on patterned surfaces. *Lab Chip.* **10**, 1182–1188 (2010).
24. Abadi, P. P. S. S. *et al.* Engineering of Mature Human Induced Pluripotent Stem Cell-Derived Cardiomyocytes Using Substrates with Multiscale Topography. *Adv. Funct. Mater.* **28**, 1707378 (2018).
25. Mashinchian, O. *et al.* Cell-imprinted substrates act as an artificial niche for skin regeneration. *ACS Appl. Mater. Interfaces.* **6**, 13280–13292 (2014).
26. Bonakdar, S. *et al.* Cell-Imprinted Substrates Modulate Differentiation, Redifferentiation, and Transdifferentiation. *ACS Appl. Mater. Interfaces.* **8**, 13777–13784 (2016).
27. Moosazadeh Moghaddam, M. *et al.* Engineered substrates with imprinted cell-like topographies induce direct differentiation of adipose-derived mesenchymal stem cells into Schwann cells. *Artif. Cells, Nanomedicine Biotechnol.* **47**, 1022–1035 (2019).
28. Kamguyan, K. *et al.* An engineered cell-imprinted substrate directs osteogenic differentiation in stem cells. *Biomater. Sci.* **6**, 189–199 (2018).
29. Braschler, Z. S. G. and M. E. and S. B. and P. R. and O. M. and S. S. and F. B. and I. U. and O. P.-S. and T. Neural priming of adipose-derived stem cells by cell-imprinted substrates.*Biofabrication*(2020).
30. Tan, L. H., Sykes, P. H., Alkaisi, M. M. & Evans, J. J. Cell-like features imprinted in the physical nano- and micro-topography of the environment modify the responses to anti-cancer drugs of endometrial

cancer cells.*Biofabrication***9**, (2017).

31. Medlock, J., Das, A. A. K., Madden, L. A., Allsup, D. J. & Paunov, V. N. Cancer bioimprinting and cell shape recognition for diagnosis and targeted treatment. *Chem. Soc. Rev.* **46**, 5110–5127 (2017).
32. Heydari, T. *et al.* Development of a Virtual Cell Model to Predict Cell Response to Substrate Topography. *ACS Nano.* **11**, 9084–9092 (2017).
33. Zhang, J., Wei, X., Zeng, R., Xu, F. & Li, X. J. Stem cell culture and differentiation in microfluidic devices toward organ-on-a-chip. *Futur. Sci. OA.* **3**, FSO187 (2017).
34. Kassis, T. *et al.* MICCS: A Fully Programmable Multipurpose Integrated Cell Culture System. bioRxiv 192047(2017). doi:10.1101/192047
35. Bao, X. *et al.* Stimulation of chondrocytes and chondroinduced mesenchymal stem cells by osteoinduced mesenchymal stem cells under a fluid flow stimulus on an integrated microfluidic device. *Mol. Med. Rep.* **17**, 2277–2288 (2018).
36. Truong, D. *et al.* A three-dimensional (3D) organotypic microfluidic model for glioma stem cells – Vascular interactions. *Biomaterials.* **198**, 63–77 (2019).
37. Huang, M., Fan, S., Xing, W. & Liu, C. Microfluidic cell culture system studies and computational fluid dynamics. *Math. Comput. Model.* **52**, 2036–2042 (2010).
38. Yazdian Kashani, S., Afzalian, A., Shirinichi, F. & Keshavarz Moraveji, M. Microfluidics for core–shell drug carrier particles – a review. *RSC Adv.* **11**, 229–249 (2021).
39. Kowsari-Esfahan, R., Jahanbakhsh, A., Saidi, M. S. & Bonakdar, S. A microfabricated platform for the study of chondrogenesis under different compressive loads. *J. Mech. Behav. Biomed. Mater.* **78**, 404–413 (2018).
40. Meyvantsson, I. & Beebe, D. J. Cell Culture Models in Microfluidic Systems. *Annu. Rev. Anal. Chem.* **1**, 423–449 (2008).
41. Wu, H. W., Lin, C. C. & Lee, G. Bin. Stem cells in microfluidics. *Biomicrofluidics.* **5**, 013401 (2011).
42. Leclerc, E. *et al.* Study of osteoblastic cells in a microfluidic environment. *Biomaterials.* **27**, 586–595 (2006).
43. Chen, H., Sun, J., Wolvetang, E. & Cooper-White, J. High-throughput, deterministic single cell trapping and long-term clonal cell culture in microfluidic devices. *Lab Chip.* **15**, 1072–1083 (2015).
44. Ong, L. J. Y. *et al.* A 3D printed microfluidic perfusion device for multicellular spheroid cultures. *Biofabrication.* **9**, 045005 (2017).
45. Dettinger, P. *et al.* Automated Microfluidic System for Dynamic Stimulation and Tracking of Single Cells. *Anal. Chem.* **90**, 10695–10700 (2018).
46. Occhetta, P. *et al.* Hyperphysiological compression of articular cartilage induces an osteoarthritic phenotype in a cartilage-on-a-chip model. *Nat. Biomed. Eng.* **3**, 545–557 (2019).
47. Smoak, M. M., Pearce, H. A. & Mikos, A. G. Microfluidic devices for disease modeling in muscle tissue. *Biomaterials.* **198**, 250–258 (2019).

48. Costantini, M. *et al.* Microfluidic-enhanced 3D bioprinting of aligned myoblast-laden hydrogels leads to functionally organized myofibers in vitro and in vivo. *Biomaterials.* **131**, 98–110 (2017).
49. Natividad-Diaz, S. L. *et al.* A combined hiPSC-derived endothelial cell and in vitro microfluidic platform for assessing biomaterial-based angiogenesis. *Biomaterials.* **194**, 73–83 (2019).
50. Bhatia, S. N. & Ingber, D. E. Microfluidic organs-on-chips. *Nat. Biotechnol.* **32**, 760–772 (2014).
51. Shi, X. *et al.* Stretchable and micropatterned membrane for osteogenic differentation of stem cells. *ACS Appl. Mater. Interfaces.* **6**, 11915–11923 (2014).
52. Kim, K. M. *et al.* Shear Stress Induced by an Interstitial Level of Slow Flow Increases the Osteogenic Differentiation of Mesenchymal Stem Cells through TAZ Activation. *PLoS One.* **9**, e92427 (2014).
53. Pavesi, A. *et al.* Controlled electromechanical cell stimulation on-a-chip. *Sci. Rep.* **5**, 1–12 (2015).
54. Park, D., Lim, J., Park, J. Y. & Lee, S. H. Concise Review: Stem Cell Microenvironment on a Chip: Current Technologies for Tissue Engineering and Stem Cell Biology. *Stem Cells Transl. Med.* **4**, 1352–1368 (2015).
55. Ong, L. J. Y. *et al.* A pump-free microfluidic 3D perfusion platform for the efficient differentiation of human hepatocyte-like cells. *Biotechnol. Bioeng.* **114**, 2360–2370 (2017).
56. Karimi, M. *et al.* Microfluidic systems for stem cell-based neural tissue engineering. *Lab Chip.* **16**, 2551–2571 (2016).
57. Woodruff, K. & Maerkl, S. J. A High-Throughput Microfluidic Platform for Mammalian Cell Transfection and Culturing. *Sci. Rep.* **6**, 1–12 (2016).
58. Hesari, Z. *et al.* A hybrid microfluidic system for regulation of neural differentiation in induced pluripotent stem cells. *J. Biomed. Mater. Res. - Part A.* **104**, 1534–1543 (2016).
59. Lyu, J. *et al.* A microfluidics-derived growth factor gradient in a scaffold regulates stem cell activities for tendon-to-bone interface healing.*Biomater. Sci.***8**, (2020).
60. Wang, K. *et al.* A microfluidic platform for high-purity separating circulating tumor cells at the single-cell level. *Talanta.* **200**, 169–176 (2019).
61. Sun, Y. S. Comparison of chip inlet geometry in microfluidic devices for cell studies.*Molecules***21**, (2016).
62. Yazdian Kashani, S. *et al.* An integrated microfluidic device for stem cell differentiation based on cell-imprinted substrate designed for cartilage regeneration in a rabbit model. *Mater. Sci. Eng. C.* **121**, 111794 (2021).
63. Montazeri, L., Bonakdar, S., Taghipour, M., Renaud, P. & Baharvand, H. Modification of PDMS to fabricate PLGA microparticles by a double emulsion method in a single microfluidic device. *Lab Chip.* **16**, 2596–2600 (2016).
64. Shokrgozar, M. A. *et al.* Biological evaluation of polyvinyl alcohol hydrogel crosslinked by polyurethane chain for cartilage tissue engineering in rabbit model. *J. Mater. Sci. Mater. Med.* **24**, 2449–2460 (2013).
65. Carlo, D., Di, Wu, L. Y. & Lee, L. P. Dynamic single cell culture array. *Lab Chip.* **6**, 1445 (2006).

66. Kavand, H. *et al.* Cell-Imprint Surface Modification by Contact Photolithography-Based Approaches: Direct-Cell Photolithography and Optical Soft Lithography Using PDMS Cell Imprints. *ACS Appl. Mater. Interfaces.* **11**, 10559–10566 (2019).

Figures

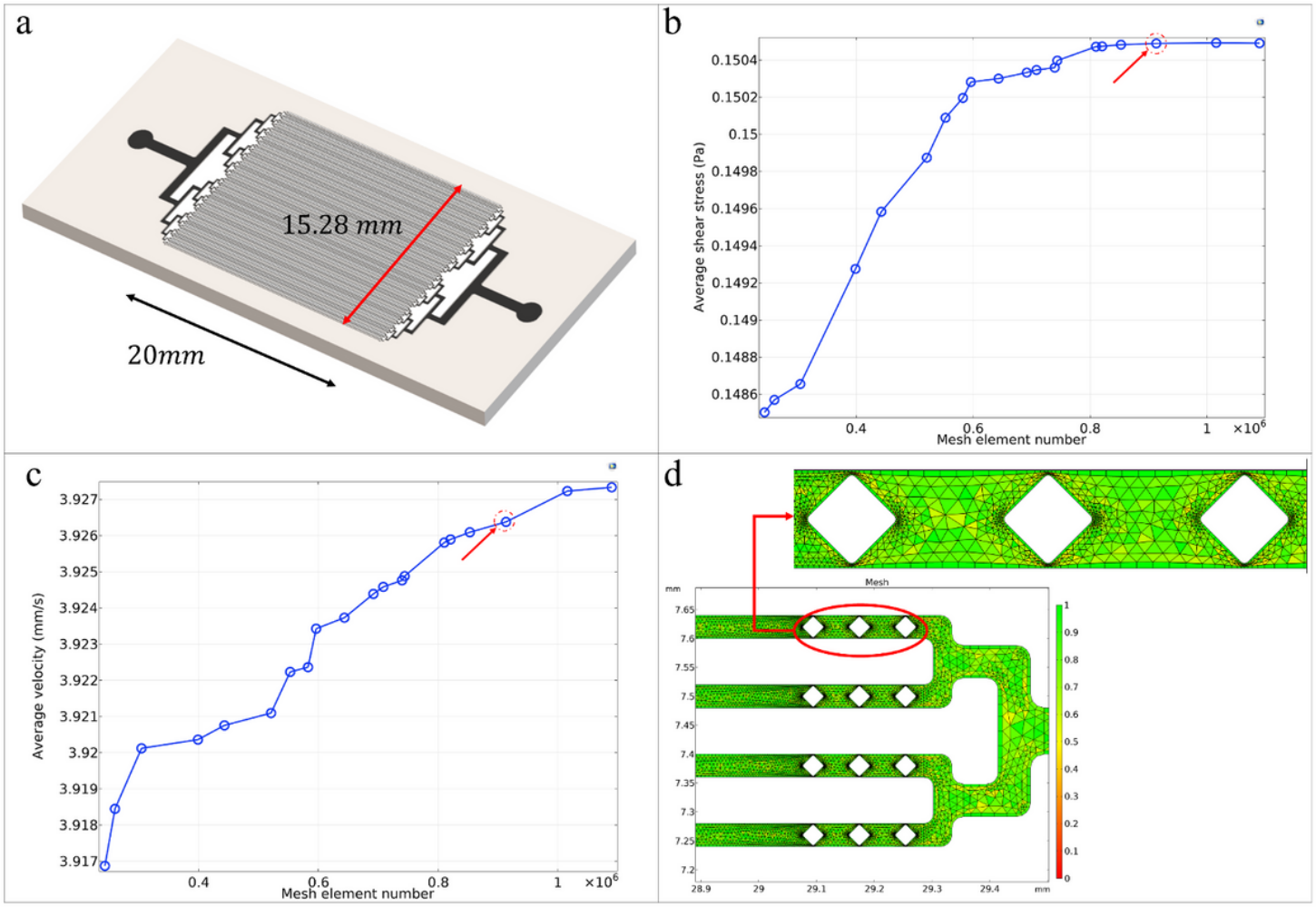

Figure 1

a) Design of the microfluidic chip with 128 40 µm microchannels. b) Convergence study for average shear stress in the microfluidic chip. c) Convergence study for average velocity microfluidic chip. d) Mesh plot around terminal microposts at the end of each microchannel. The color bar shows the mesh quality.

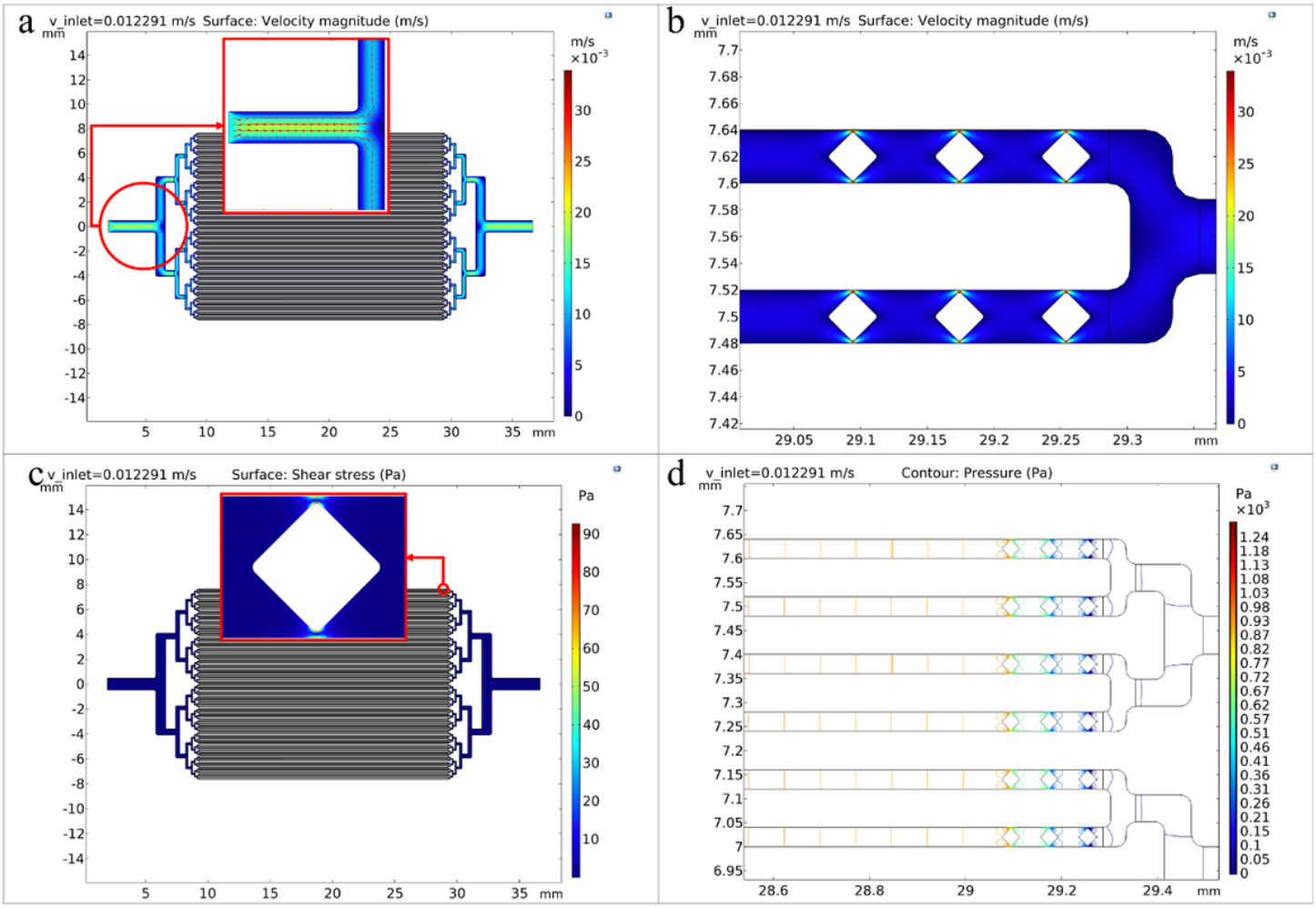

Figure 2

a) Velocity profile in the microfluidic chip. b) Velocity profile in the microfluidic chip around terminal microposts. c) Shear stress profile in the microfluidic chip. The shear stress profile around a terminal micropost is zoomed. d) Pressure contour in the microfluidic chip around terminal microposts. All data were obtained for the microfluidic chip with 40 μm microchannels.

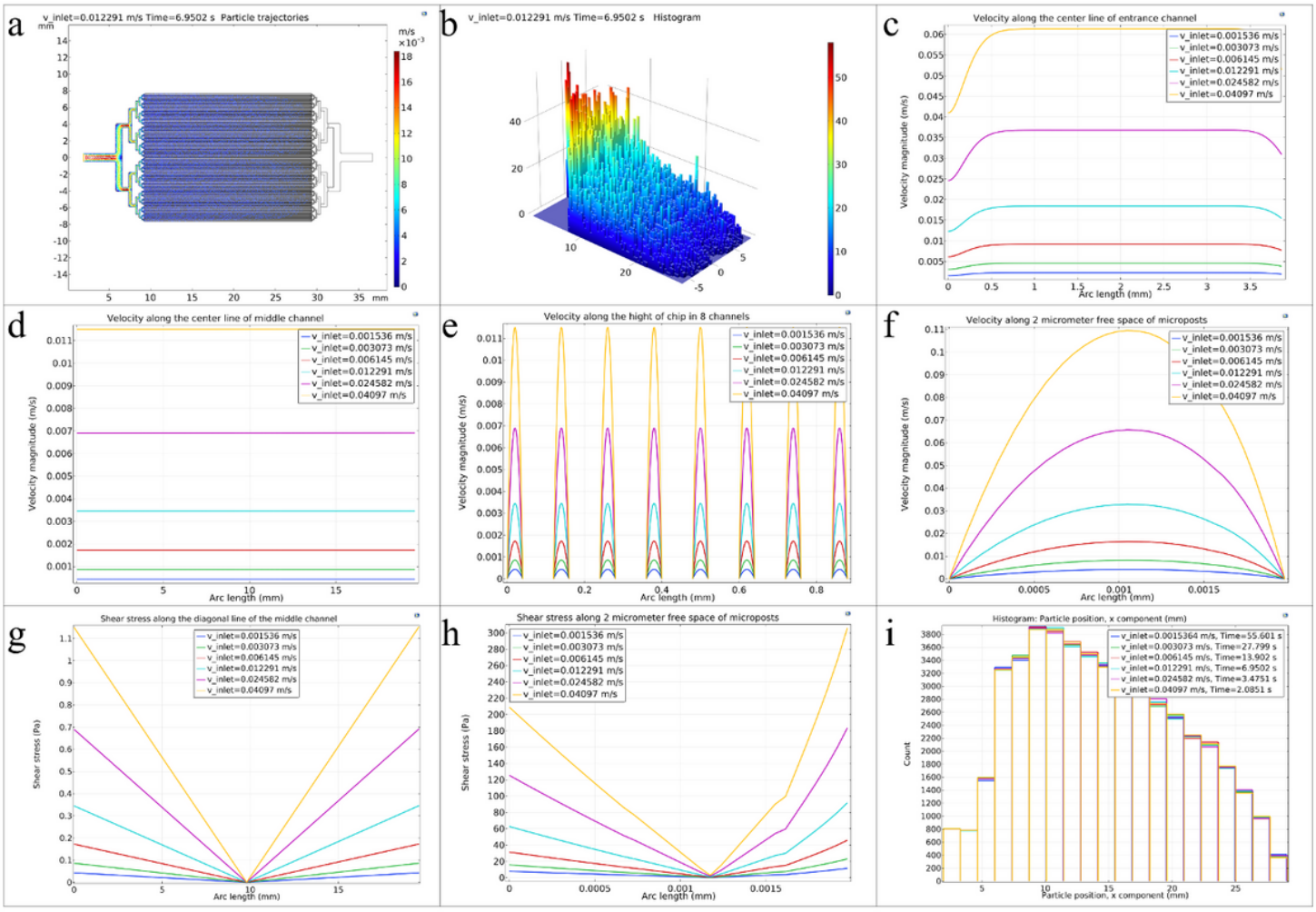

Figure 3

a) Cell trajectories in the microfluidic chip when the first cells reach the terminal microposts. The cells' color indicates their velocity (m/s). A scale factor of 4.9 is used for cell radius for better demonstration. b) Histogram plot of cells distribution along the microfluidic chip when the first cells reach the terminal microposts. c) Velocity changes along the input channel's centerline. d) Velocity changes along a cut line on the centerline (before reaching the central microchannel's terminal microposts). e) Velocity changes along the microfluidic chip's height in eight consecutive microchannels. f) Velocity changes in the direction of 2 μm vertical free distance between the micropost and the channel wall. g) Shear stress changes along a diagonal cut line from the central microchannel's bottom-left point to its top-right point (before reaching the central microchannel's terminal microposts). h) Shear stress changes in the direction of 2 μm vertical free distance between the micropost and the channel wall. i) Histogram of cell position along the microfluidic chip. All data were obtained for the microfluidic chip with 40 μm microchannels, and Fig. 3.c-i were obtained for different inlet velocities in the microfluidic chip.

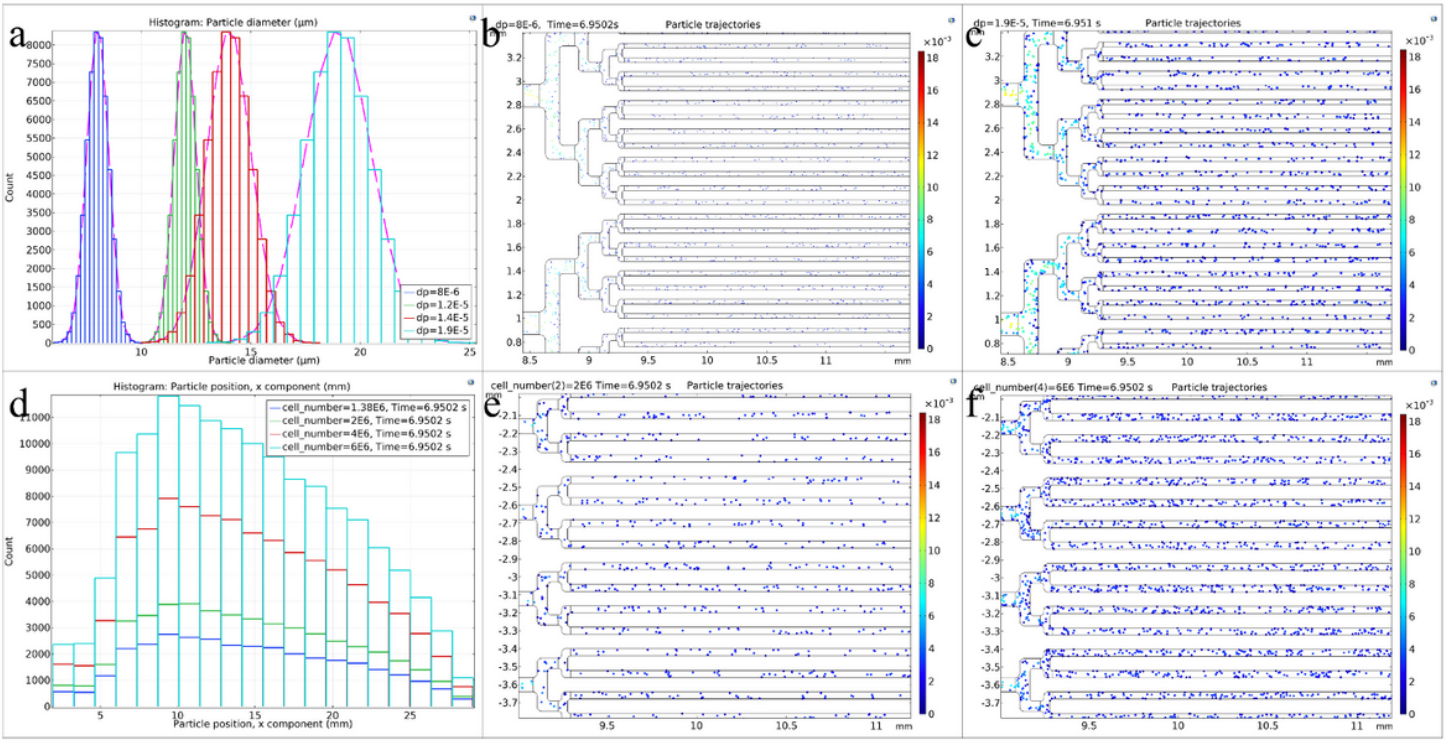

Figure 4

a) Normal distribution of cell size for cells with average diameters of 8, 12, 14, and 19 μm in the microfluidic chip. b) 8 μm diameter cell trajectories in the microfluidic chip. c) 19 μm cell trajectories in the microfluidic chip. d) Histogram of cell position along the microfluidic chip for different cell numbers in a constant volume of cell culture medium. e) Cell trajectories in the microfluidic chip for a cell concentration of 2*106 cell/170 μl cell culture medium. f) Cell trajectories in the microfluidic chip for a cell concentration of 6*106 cell/170 μl cell culture medium. All data were obtained for the microfluidic chip with 40 μm microchannels.

Figure 5

a) The schematic of the cell-imprinted-based integrated microfluidic device fabrication procedure. b) 40µm microchannels of the microfluidic chip are almost filled with HUVEC cell line after injection with a syringe pump. c) The regular pattern of HUVEC cell lines transferred to the cell-culture plate. d) 25µm microchannels of the microfluidic chip are almost filled with L929 cell line after injection with a syringe pump. e) The regular pattern of L929 cell lines transferred to the cell-culture plate.

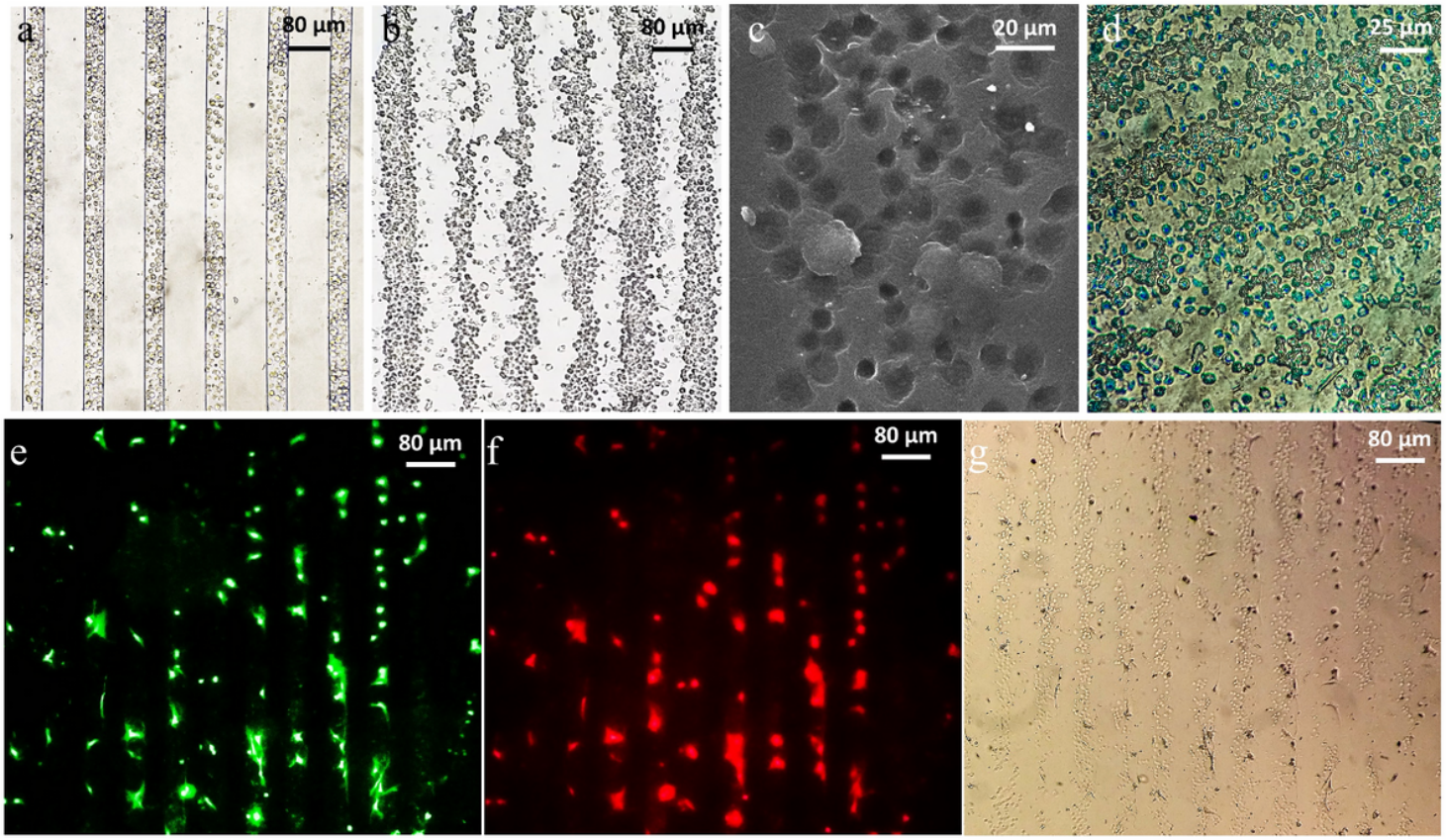

Figure 6

a) 40µm microchannels of the microfluidic chip almost filled with chondrocytes. b) The regular pattern of chondrocytes transferred to the cell-culture plate. c) The chondrocyte-imprinted substrate SEM image prepared by a microfluidic chip with 40µm microchannels. d) Stained ADSCs cultured in a 25µm microfluidic chip on the cell-imprinted substrate with alcian blue. e) Phalloidin staining of actins in cultured ADSCs in a microfluidic chip on the cell-imprinted substrate. f) Immunostaining of ADSCs cultured in a microfluidic chip on the cell-imprinted substrate with fluorescent AlexaFluor488 labeled wheat germ agglutinin (WGA). g) Optical microscopy of ADSCs cultured in a microfluidic chip on the cell-imprinted substrate.

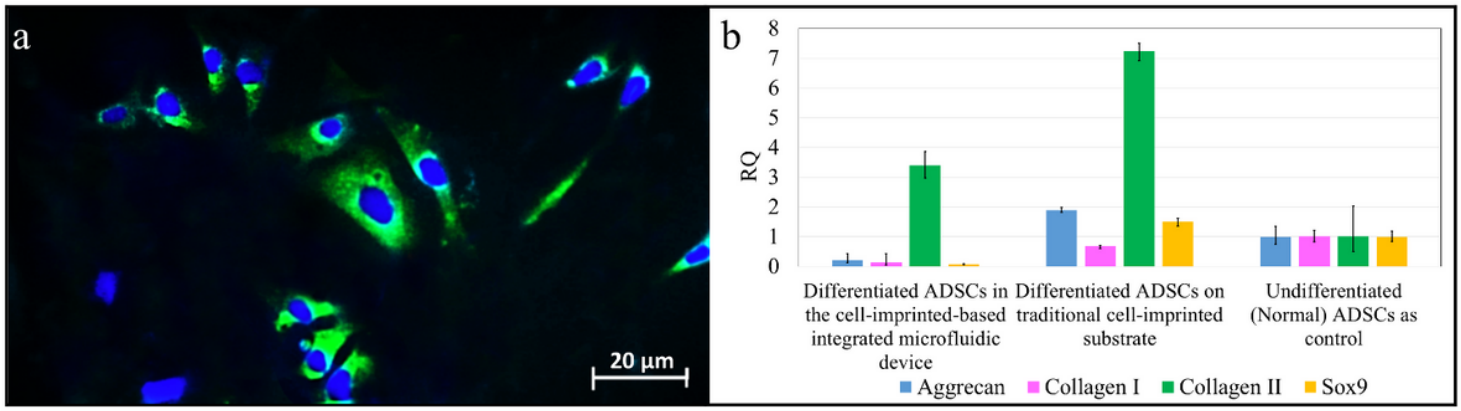

Figure 7

a) Stained ADSCs in a 25μm microfluidic chip on the cell-imprinted substrate with collagen II (green) and DAPI (blue) for the nucleus. b) Quantitative real-time PCR analysis: gene expression profile of differentiated ADSCs in the cell-imprinted-based integrated microfluidic device and on the traditional cell-imprinted substrate and freshly isolated ADSCs which were grown on standard cell culture flasks as control; different genes (aggrecan, collagen I, collagen II, and sox9) are expressed relatively.

Supplementary Files

This is a list of supplementary files associated with this preprint. Click to download.

- Graphicalabstract.tif
- afterchangessupplementaryinformation.docx
- video1rangi.rar
- video2.mp4